

1 **Transcranial direct current stimulation alters functional network structure in humans**

2

3

4 M. Ruttorf^{1*}, S. Kristensen^{2,3}, L.R. Schad¹, J. Almeida^{2,3*}

5

6

7 ¹ Computer Assisted Clinical Medicine, Medical Faculty Mannheim, Heidelberg University,
8 Germany

9 ² Proaction Laboratory, Faculty of Psychology and Educational Sciences, University of
10 Coimbra, Portugal.

11 ³ Faculty of Psychology and Educational Sciences, University of Coimbra, Portugal.

12

13

14 *Correspondence: michaela.ruttorf@medma.uni-heidelberg.de (M.R.),

15 jorgecbalmeida@gmail.com (J.A.)

16

17

18 Keywords: transcranial direct current stimulation, functional magnetic resonance imaging,

19 network analysis, graph theory, tool network

20

21

22

23

24

25

26

27 **Abstract**

28 Transcranial direct current stimulation (tDCS) is routinely used in basic and clinical research,
29 but its efficacy has been challenged on a methodological and statistical basis recently. The
30 arguments against tDCS derive from insufficient understanding of how this technique
31 interacts with brain processes physiologically. Because of its potential as a central tool in
32 neuroscience, it is important to clarify whether and how tDCS affects neuronal activity. Here,
33 we investigate influences of offline tDCS on network architecture measured by functional
34 magnetic resonance imaging. Our results reveal a tDCS-induced reorganisation of a
35 functionally-defined network that is dependent on whether we are exciting or inhibiting a
36 node within this network, confirming in a functioning brain, and in a bias free and
37 independent fashion that tDCS influences neuronal activity. Moreover, our results suggest that
38 network-specific connectivity has an important role in defining the effects of tDCS and the
39 relationship between brain states and behaviour.

40

41 Transcranial direct current stimulation^{1,2,3,4,5} (tDCS) has been widely used in the
42 neurosciences^{6,7,8,9} for decades. This is so because interfering techniques like tDCS that are
43 assumed to directly modulate neuronal activity are extremely promising for both basic and
44 applied research as they allow for addressing research questions on the causal relationships
45 between brain states and behaviour^{10,11,12}. However, the efficacy of tDCS has been put into
46 question recently^{13,14,15,16,17} on a methodological and statistical basis. It is thus central to
47 have a closer look at the effects of tDCS on brain activity. In our previous publication⁵, we
48 have already shown by whole-brain functional magnetic resonance imaging (fMRI) analyses
49 that offline tDCS locally affects neuronal responses in a single brain region in accordance
50 with stimulation polarity (i.e., inhibition or excitation). Nevertheless, the global effect of
51 tDCS on functional brain networks in humans is still not well understood^{18,19}. Based on our
52 previous whole-brain fMRI results⁵ and on the detailed work on living macaques by Krause

53 et al. (2017)²⁰, we decided – as a second step - to investigate, in humans, the impact of tDCS
54 on a functional brain network. We did so using the same experimental settings as before⁵.
55 There are certain key methodological issues related to the effect of tDCS in the brain that are
56 currently unsolved^{21,13,12}. These include understanding the technique’s (i) functional
57 focality, i.e. is tDCS limited to local effects on the stimulated area, or do the effects also
58 transfer more globally to the network level as pointed out by Krause et al (2017)²⁰; (ii)
59 specificity of stimulation, i.e. is tDCS-induced interference dependent on general processes
60 such as the spatially wide expansion of the electrical field²², or is it dependent on more
61 neuronally-specified processes such as functional connectivity between regions; or (iii)
62 modulatory effects, i.e. how does tDCS modulate functional connectivity between brain
63 regions. Up to now, there are only two studies evaluating the effect of tDCS on the structure
64 of underlying functional brain networks in depth by means of graph theory: one uses tDCS in
65 combination with resting-state fMRI²³, and the other combines tDCS with
66 electroencephalography²⁴. Importantly, none of these examined topology changes in
67 functional brain networks in detail. For this reason and because cognitive functions rely on the
68 processes happening within networks of functionally-connected brain regions rather than on
69 local and isolated areas, we look at how tDCS affects neuronal organisation using a task-
70 based fMRI experiment after applying of offline tDCS. We did so because: (i) task
71 performance enhances neuronal activity resulting in functional connectivity between relevant
72 brain areas being more reliable in terms of graph theory metrics²⁵; (ii) tDCS preferentially
73 modulates active neuronal networks, when compared to inactive networks sharing the same
74 anatomical space (activity-selectivity approach)²⁶; and (iii) offline tDCS allows us to map the
75 spatio-temporal patterns of functional reorganisation at the systems level²⁷.

76

77

78

79 **Experimental Layout**

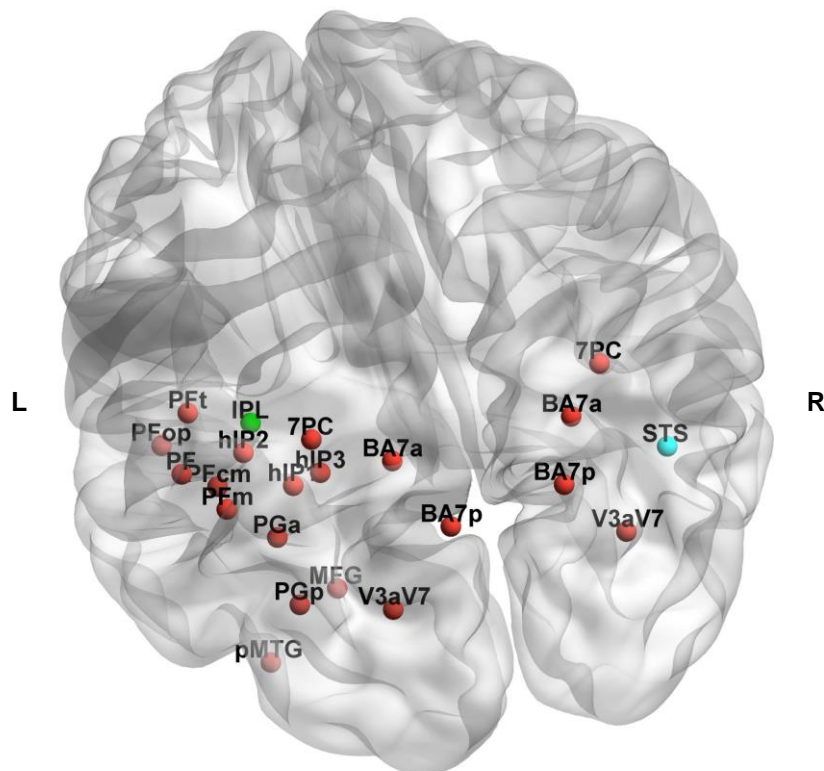
80 We combined tDCS with a task-based paradigm in fMRI using a repeated measures design
81 (see Methods for more details). We asked a group of ten individuals to participate in four
82 experimental sessions, resulting in a total of 40 sessions. Each session was separated by at
83 least one week. In the first session, participants went through the fMRI experiment only – as
84 control session – whereas in the second to fourth sessions participants were first subject to
85 tDCS stimulation outside the MR scanner that was immediately followed by the fMRI
86 measurement. The fMRI paradigm consisted on passively watching pictures of tools, animals,
87 faces and places. The tDCS sessions consisted of anodal (typically thought to increase
88 neuronal excitability) or cathodal (typically thought to decrease neuronal excitability)^{28,19}
89 stimulation to either the left Inferior Parietal Lobule (IPL) or the right Superior Temporal
90 Sulcus (STS). This resulted in four experimental within-participant groups: anodal stimulation
91 on IPL (AnoIPL), cathodal stimulation on IPL (CatIPL), cathodal stimulation on STS
92 (CatSTS) and control (Ctrl). We chose the left IPL and right STS as target areas because they
93 are highly accessible to the tDCS stimulation technique. Moreover, we have already shown
94 that IPL responds more to images of tools than images of stimuli from other categories (see
95 results in ⁵), whereas STS does not³⁰. This is important because by using STS we obtained a
96 tDCS “sham” group to compare tDCS to IPL with – additionally to the control group that
97 serves as ground truth without stimulation. Contrary to classical sham procedures, here
98 participants receive active stimulation to an alternative location to counter doubts which arose
99 recently^{31,13} concerning the ability to distinguish classical sham from active stimulation.

100 We decided to concentrate on brain areas that are dedicated to the processing of tool items
101 (i.e., the tool network^{5,32,33}), which left IPL is an exemplary constituent, because effects of
102 tDCS depend on the cognitive/neural processing participants are engaged in – i.e., because
103 this network would be actively processing the tool stimuli presented in our experiment, we
104 could better test the effects of tDCS over this network. We selected 18 regions of interest

105 (ROIs) that have been associated with tool processing^{29,34,35}. The location of the ROIs can
106 be seen in Figure 1 using BrainNet Viewer software³⁶ (Version 1.53) as red spheres placed
107 on the ICBM-152 template³⁷. The location corresponds to the ROIs' centre coordinates listed
108 in Table 1. Brain networks demonstrate hierarchical modularity (or multi-scale modularity) -
109 i.e. each module contains a set of sub-modules that contains a set of sub-sub-modules, etc³⁸.
110 Object recognition – and thereby the tool network as well – is organised in a modular way
111 comparable to colour vision which is shown to be automatic, effortless and informationally
112 encapsulated³⁹. Thus, we treated the tool network as a modular network with a subset of
113 highly functional-connected nodes. Keeping this in mind, we are able to test whether tDCS
114 can induce reorganisation over a functional network in the brain, and specifically here over
115 the tool network, beyond the known local effects over the stimulated area as reported in our
116 previous publication⁵.

117

118



119

120 **Figure 1: Location of the regions of interest analysed.** Coloured in red are the regions of
121 interest (ROIs) within the tool functional network according to centre coordinates and labels
122 given in Table 1. The location of the stimulation sites is shown either in green (Inferior
123 Parietal Lobule – IPL) or in blue (Superior Temporal Sulcus – STS). L/R denotes the left and
124 right hemisphere, respectively. A video with 360° view of the location of the ROIs is
125 available as Supplementary Information.

126

127 **Graph Theory Analysis**

128 A graph is mathematical description of a network consisting of nodes N (here: the ROIs
129 selected) and edges k (here: functional “links” between pairs of ROIs). Below, we refer to
130 graphs explicitly because this does not make any assumptions on the nature of the edges but
131 rather emphasises the aspect of mathematical modelling because “network” generally refers to
132 real-world connected systems⁴⁰. We analysed weighted undirected graphs averaged per group
133 (see Methods for details of graph construction) using Brain Connectivity Toolbox⁴¹
134 implemented in MATLAB R2013a (The MathWorks Inc., Natick, MA, USA). Because we
135 were interested in changes in underlying network architecture in the brain between
136 experimental groups we looked at topological graph metrics as community structure and
137 participation coefficients primarily. After graph construction, we checked for N,k -dependence
138 (see Methods). The number of nodes stays constant ($N = 18$) in all experimental groups, the
139 number of edges is almost equal between groups ($\bar{k} = 150$, $\Delta k = \pm 2$). Using a repeated
140 measures design, we were only interested in changes between experimental groups. So, we
141 kept the resulting graphs while considering the gain or loss of an edge as an effect of the
142 stimulation (tDCS).

143

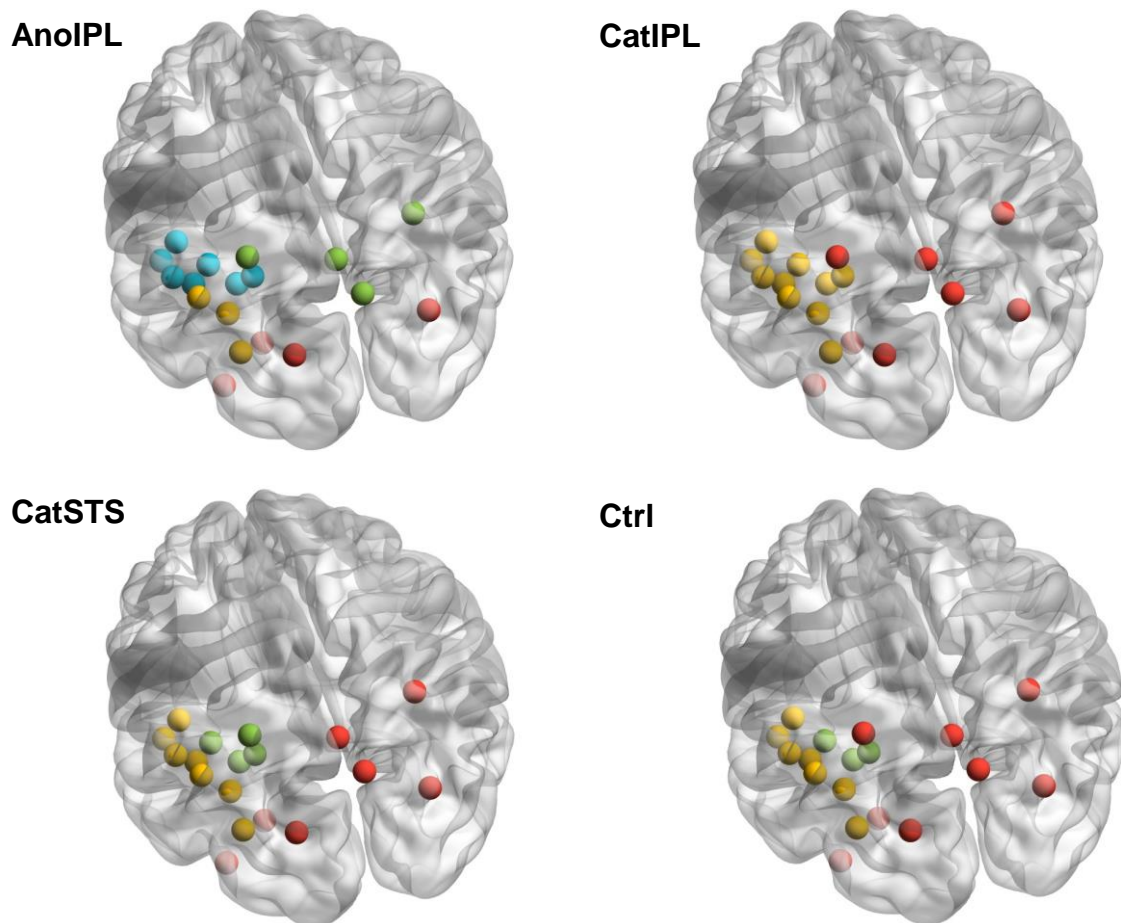
144

145

146 **Community Structure**

147 Community structure has been identified as a sensitive marker for organisation in brain
148 networks⁴². Community structure analysis detects the groups of regions more densely
149 connected between them than expected by chance. The resulting group-level community
150 structure was visualised by assigning a different colour to each community (see Figure 2).
151 This was then displayed by overlaying spheres coloured by community affiliation on the
152 ICBM-152 template as done in Figure 1.

153

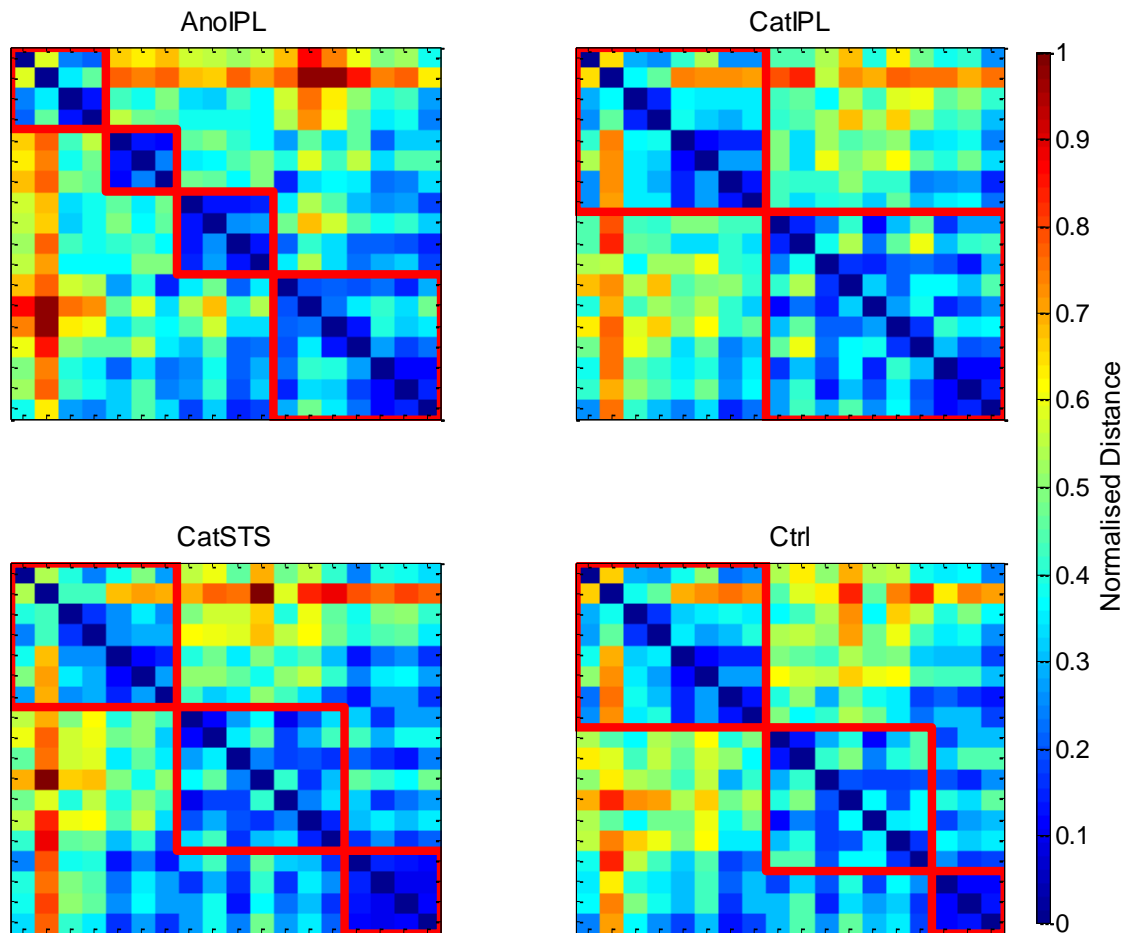


154

155 **Figure 2: Community structure of the tool network.** Within the four experimental groups
156 (AnoIPL, CatIPL, CatSTS and Ctrl), resulting community structures of the tool network are
157 shown. Colours denote different communities; red indicates community I, yellow community
158 II, green community III and blue community IV. Angle of vision kept as in Figure 1. Location
159 of the spheres visualised according to centre coordinates given in Table 1.

160

161 The values of modularity Q corresponding to the community structures shown in Figure 2 are
162 almost identical ($\Delta Q = \pm 0.02$). There are three communities in the Ctrl and CatSTS
163 experimental groups, two in CatIPL experimental group and four in AnoIPL experimental
164 group. The communities in Ctrl and CatSTS experimental groups differ minimally from each
165 other. One node changed community assignment (from community III to community I). In
166 AnoIPL experimental group, the community structure intensifies to four whereas in CatIPL
167 experimental group the community structure relaxes to two. We controlled for possible
168 limitations⁴³ relevant to our experimental layout: the results shown in Figure 2 are neither
169 subject to resolution limit of the objective function⁴⁴ nor dependent on the method used to
170 average the correlation coefficients (see Methods for more details). Furthermore, we overlaid
171 the community structure for each experimental group on their averaged weighted temporal
172 correlation matrix before converting to absolute values to verify that negative edge weights
173 are sparser within and denser between communities found⁴⁵. Likewise, we overlaid the
174 community structure for each experimental group on their distance matrix (see Methods) to
175 re-examine that distances within communities are smaller than between communities as
176 shown in Figure 3. We show that the number of communities changed depending on
177 stimulation site and polarity of tDCS. While there is almost no difference in community
178 affiliation when stimulating STS which does not belong to the tool network, there are clear
179 polarity-dependent effects when stimulating IPL.



180

181 **Figure 3: Plots of distance matrices with community structure on top.** For the four
 182 experimental groups (AnoIPL, CatIPL, CatSTS and Ctrl), normalised distance matrices
 183 grouped by communities are shown. The borders of the communities are marked by thick red
 184 lines. The colour bar indicates the normalised distance between nodes. The distance is less
 185 within communities than between communities throughout experimental groups in all
 186 communities found.

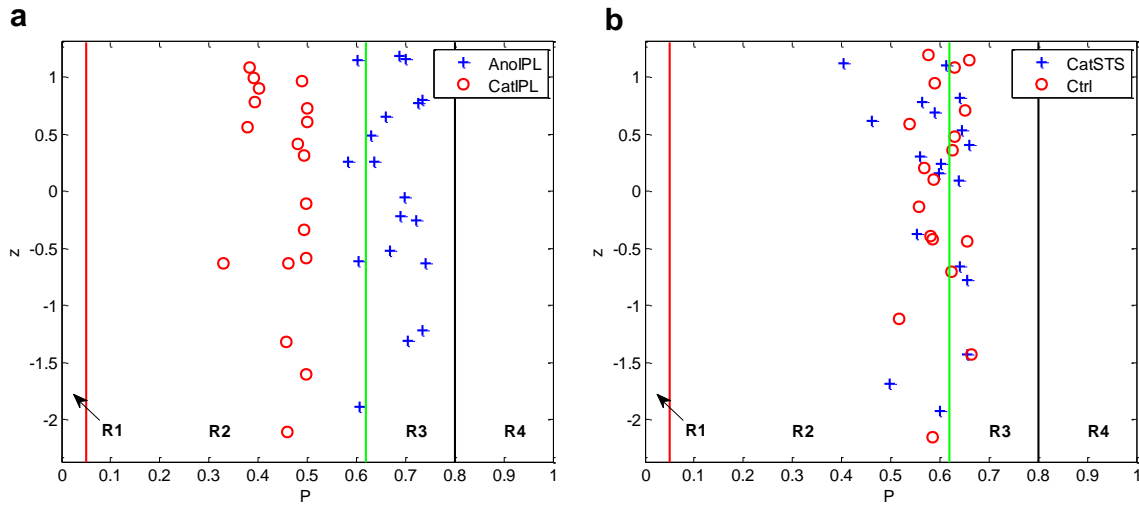
187

188 **Participation Coefficient**

189 While the within-module degree z score defines the role of a node in its own community, the
 190 participation coefficient P is a feature of each node's connectivity relative to the community
 191 structure of the entire network⁴⁶. Nodes with a low value of P share connections with other
 192 members of the same community, whereas those with a high P value serve as connectors

193 between communities. In Figure 4, the P values for the four experimental groups are plotted
 194 in the P - z parameter plane (see Methods for details).

195



196

197 **Figure 4: Plots of within-module degree z against participation coefficient P .** For the four
 198 experimental groups (AnoIPL, CatIPL, CatSTS and Ctrl), P - z -plots are shown. The borders of
 199 the different regions (R1 – R4, see Methods) are marked by lines. There is a clear difference
 200 in distribution between groups AnoIPL and CatIPL (a) while there is no difference between
 201 groups CatSTS and Ctrl (b).

202

203 There is a clear difference visible in the distributions of P values between CatIPL and AnoIPL
 204 experimental groups (Figure 4 (a)) while there seems to be no difference in the other two
 205 experimental groups (Figure 4 (b)). Therefore, we analysed the differences in P distributions
 206 using the Wilcoxon signed-rank test as implemented in MATLAB R2013a. The one-tailed
 207 Wilcoxon signed-rank test with $\alpha = 0.01$ shows a significant difference in AnoIPL > CatIPL
 208 ($z_{wilcoxon} = 3.70, p \ll 0.01$), AnoIPL > CatSTS ($z_{wilcoxon} = 3.09, p \ll 0.01$), AnoIPL > Ctrl
 209 ($z_{wilcoxon} = 2.92, p \ll 0.01$), CatIPL < CatSTS ($z_{wilcoxon} = -3.66, p \ll 0.01$) and CatIPL < Ctrl
 210 ($z_{wilcoxon} = -3.70, p \ll 0.01$). There was no significant difference using the two-tailed
 211 Wilcoxon signed-rank test with $\alpha = 0.01$ in CatSTS \neq Ctrl ($z_{wilcoxon} = -0.85, p > 0.39$).

212 Compared to both control experimental groups, more nodes in the AnoIPL experimental
213 group jumped to region R3 while those of the CatIPL experimental group fell back
214 completely to region R2. Finally, we analysed the differences in z distributions as well. There
215 was no significant difference using the two-tailed Wilcoxon signed-rank test with $\alpha = 0.01$
216 between groups: AnoIPL \neq CatIPL ($z_{wilcoxon} = 0.24, p > 0.81$), AnoIPL \neq CatSTS ($z_{wilcoxon} =$
217 $0.20, p > 0.84$), AnoIPL \neq Ctrl ($z_{wilcoxon} = -0.20, p > 0.84$), CatIPL \neq CatSTS ($z_{wilcoxon} = 0.11, p$
218 > 0.91), CatIPL \neq Ctrl ($z_{wilcoxon} = 0.02, p > 0.98$) and CatSTS \neq Ctrl ($z_{wilcoxon} = 0.37, p > 0.71$).
219 The role of nodes within their community (z value) does not differ significantly in all
220 experimental groups. The role of nodes to other communities (P value) changed depending on
221 the kind of stimulation. There was no change compared to Ctrl in the CatSTS experimental
222 group. But in the AnoIPL experimental group, the community structure intensifies and so do
223 the edges between communities. The four modules are more densely connected, the node
224 roles jumped from region R2 (lower P values) to region R3 (higher P values) having more
225 edges to other communities as compared to both control groups. The opposite is the case in
226 the experimental group CatIPL where the module structure relaxes and so do the node roles.
227 They drop completely to region R2 (lower P values) having less edges between communities
228 than in both control experimental groups.

229

230 **Discussion**

231 Here we show that tDCS to one node of a functional network affects the network architecture
232 as a whole. Altogether, the results presented here and in our previous publication⁵ provide a
233 proof of principle that tDCS – delivered through the scalp using currents of 2 mA – can
234 influence neuronal activity in humans. Moreover, they suggests that the effects of tDCS may
235 arise from changed communication patterns (and not just local modulation of signal) that are
236 modified by stimulation polarity and from altered functional connectivity between brain areas.

237 Crucially, our data shed light to some of the unresolved issues regarding the effects of tDCS
238 at systems level. Namely, that: (i) tDCS is not limited to a local effect on the stimulated area,
239 but exerts polarity-specific effects on the topology of the functional network attached; (ii) this
240 effect is, if anything, only minimally affected by non-specific spread of the tDCS induced
241 electrical field, but is rather dependent on network-specific processing of information; and
242 (iii) at an intermediate scale, tDCS modulates functional connectivity by modular
243 reorganisation.

244 Our results also show that in anodal tDCS the community structure in a regional and task-
245 related network that is attached to the stimulation site intensifies and this leads to more edges
246 between these communities. The existence of some edges between nodes in different
247 communities acts as topological short-cuts³⁸. This is in line with the results by Polania et al.
248 (2011)²³ who came to the conclusion that anodal tDCS increased the functional coupling
249 between left somatomotor cortex (SM1) and neighboured topological regions (left premotor,
250 motor and left parietal cortex) while the number of direct functional connections from left
251 SM1 to topologically distant grey matter voxels decreased significantly. Interestingly, our
252 results contradict Mancini et al.²⁴ who stated that although tDCS is able to change network
253 properties, it does not seem to affect the topological organisation of brain activity at a global
254 level - which is not the case, as we show here.

255 Our results in the human brain are in line with those of Krause et al. (2017)²⁰ who came to
256 the conclusion that tDCS, in the primate brain, acts by modulating functional connectivity
257 between brain areas. Despite the fact these authors showed – in agreement with Vöröslakos et
258 al. (2018)¹³ – that in standard tDCS protocols, the electric field reaching the brain is too weak
259 to alter the firing rate of neurons, they also detected a significant increase in anodal
260 stimulation in the local field potential power and coherence in the targeted region when
261 inspecting the effect of tDCS within the same protocols on the brain of living macaques – an

262 ideal model system because of their thick, dense skull and gyrencephalic cortex similar to
263 humans.

264 Finally, our data are highly consistent with the proposal that effects of tDCS depend on the
265 level of ongoing activation in the particular functionally-defined target network⁴⁷ – when we
266 stimulated a node from another functionally-defined network (i.e., STS) we do not see any
267 tDCS stimulation effects on the tool network.

268 To conclude, our findings confirm that tDCS influences neuronal activity in humans in a
269 polarity-specific way, and does so in an experimental condition where participants are blind to
270 the polarity of the tDCS stimulation, the measurement (BOLD signal) is bias free in what
271 concerns the status of tDCS – i.e., within a completely independent analysis – and the neural
272 tissue is alive and is engaged in processing incoming stimuli. Moreover, we also show that the
273 flow of information within a functionally-isolated network is altered in a polarity-specific way
274 and that this may be partially the locus of the causal relation between brain states and
275 behaviour.

276

277 **Methods**

278 **Data Acquisition and Pre-processing**

279 We performed a consecutive offline tDCS/fMRI experiment on ten healthy right-handed
280 students of the University of Coimbra (equal number of females and males) at a 3T
281 MAGNETOM Trio whole-body MR scanner (Siemens Healthineers, Erlangen, Germany).
282 The study adhered to the Declaration of Helsinki and was approved by the Ethic Committee
283 of the Faculty of Medicine, University of Coimbra, Portugal. All participants gave written
284 informed consent after a detailed description of the complete study. Participants went through
285 four experimental sessions: a control session where they participated only in the fMRI
286 experiment; a tDCS anodal session on IPL followed immediately by the fMRI experiment; a
287 tDCS cathodal session on IPL followed immediately by the fMRI experiment; and a tDCS

288 cathodal session on STS followed immediately by the fMRI experiment. All participants went
289 through the control session first. The order of the tDCS sessions was counterbalanced across
290 participants. Each session was separated by at least a week. During the fMRI experiment, the
291 participants viewed pictures passively in an object processing paradigm where we presented
292 images of tools, animals, famous faces, and famous places in a miniblock design⁴⁸ (each
293 miniblock was restricted to a category). Within each run, miniblocks were pseudo-
294 randomised; all participants completed five runs of this experiment which resulted in
295 recording 455 functional volumes per session. Further information about paradigm
296 presentation, fMRI data acquisition and tDCS methodology is given in great detail in our
297 previous publication⁵ where we used the same experimental settings.

298 For analysis of functional brain networks, we extracted the overall mean time series from each
299 of 18 brain regions known to be part of the tool network^{29,34,35,49,50,51,52} (see Table 1)
300 using a BrainVoyager software (Brain Innovation, Maastricht, The Netherlands) adapted
301 Anatomy Toolbox⁵³. Before extraction of the time series, the functional volumes were pre-
302 processed using BrainVoyager QX 2.8 applying slice-time and 3D motion correction,
303 normalisation to Talairach space⁵⁴, and z-normalisation. The time series were high-pass
304 filtered (0.008 Hz) to remove low-frequency scanner drift before constructing functional brain
305 networks.

306

307 **Construction of Functional Brain Networks**

308 Each of the 18 ROIs selected above represents a single node in the resulting functional
309 network. From the overall mean time series, we then obtained a temporal correlation matrix
310 (size 18 x 18) for each participant by computing the Pearson partial correlation coefficients
311 with controlled variables as implemented in MATLAB R2013a between time series of every
312 pair of ROIs, while controlling for effects of noise. As covariates of non-interest for noise
313 correction, we grouped the mean time series from white matter and cerebrospinal fluid

314 extracted for each participant individually along with each participant's motion parameters
315 derived from the realignment step in pre-processing and the effects of the paradigm. The
316 covariate of the paradigm effect was generated by convolving the box-car functions of
317 paradigm conditions with the standard hemodynamic response function implemented in
318 Statistical Parametric Mapping software (SPM12 (v6685), Wellcome Trust Centre for
319 Neuroimaging, Institute of Neurology, University College London, UK) and was used to
320 remove signal fluctuations of paradigm conditions from the time series. For each temporal
321 correlation calculated, a p-value is given based on Student's t distribution. To minimise the
322 number of false-positives, we used a significance level of $p < 0.002$ (Bonferroni correction) to
323 threshold the temporal correlation matrix of each participant. The remaining correlations can
324 be interpreted as connections or edges between the nodes of the functional network. Here, the
325 values of the correlation coefficients serve as edge weights showing the strength of a relation.
326 While binary values enhance contrast they may also hide important information as edge
327 weights below or above threshold may vary substantially between groups. Weighted graph
328 analysis preserves this information. In our analyses, to avoid negative edge weights we
329 converted them to absolute values because we were interested in any changes between the
330 four experimental groups. It was shown elsewhere⁵⁵ that linearly mapping the weight range [-
331 1,1] to [0,1] kept the topology metrics of functional brain networks.

332

333 **Averaging correlation coefficients**

334 There are at least three different methods to average correlation coefficients: (i) calculation of
335 arithmetic mean of rs which is known to underestimate the true sample mean, (ii) Fisher's z-
336 transform and inverse Fisher's z-transform before and after averaging which is known to
337 overestimate the true sample mean⁵⁶ and (iii) Olkin-Pratt estimator⁵⁷ which is supposed to
338 be least biased. Because of our sample sizes ($N \leq 10$) which are known to be affected by
339 bias⁵⁸ most, we calculated averaged correlation matrices for each group using all three

340 methods. Then, we computed all graph theory metrics listed below with the three group
341 means averaged differently. There were no qualitative differences in the results. The choice of
342 method had no noteworthy influence. For further analysis, we used the Olkin-Pratt estimator
343 because it is recommended for averaging correlations either across samples or over repeated
344 measures within sample⁵⁹.

345

346 **Graph Theory Metrics**

347 In general, networks (or graphs) are represented as sets of nodes N and edges k . Graphs are
348 said to be unweighted if edges are either only present or absent – or weighted if edges are
349 assigned weights. Graphs are undirected if edges do not contain directional information and
350 directed if they do. Here, we analysed weighted undirected graphs by means of graph theory
351 using the Brain Connectivity Toolbox⁴¹ (BCT, version 2017-01-15). All graphs analysed are
352 connected graphs. Graph theory metrics depend on the number of N and k ⁶⁰ (N,k -
353 dependence) as well as on the choice of correlation matrix and edge weights⁶¹. N,k -
354 dependence can have two effects on graph theory metrics: (i) true effects are masked by
355 opposite effects and (ii) significant effects are introduced. Here, we have primarily looked at
356 graph theory metrics that are less sensitive to changes in N and k like topological metrics.
357 First, we compared the graphs of the four groups concerning number of edges to address N,k -
358 dependence of graph metrics. The number of nodes (here: 18) stays constant throughout
359 groups. Then, we looked at topological metrics such as modularity, community structure,
360 within-module degree z score, participation coefficient and distance.

361

362 *Degree*: Node degree is the number of edges connected to a node. During calculation of node
363 degree using BCT, weight information on edges is discarded⁶⁰.

364

365 *Modularity*: The modularity Q measures the goodness with which a graph is optimally
366 partitioned into functional subgroups or communities. For weighted graphs, modularity is
367 defined as⁶²

$$Q = \frac{1}{2m} \sum_{i,j} \left[A_{ij} - \frac{k_i k_j}{2m} \right] \delta(c_i, c_j)$$

368 with A_{ij} : weight of edge between i and j , $k_i = \sum_j A_{ij}$: sum of weights of edges attached to vertex
369 i , c_i : community vertex i is assigned to, $\delta(x,y)$ is 1 if $x = y$ and 0 otherwise and $m = 1/2 \sum_{ij} A_{ij}$.
370 Being a scalar value, Q lies in the interval $[-1,1]$, theoretically. If the fraction of within-
371 community edges is no different from what is expected for the randomised network, then Q
372 will be zero. Nonzero values indicate deviations from randomness. Q measures the density of
373 links inside communities compared with links between communities. In this context, the
374 modularity Q is used as an objective function to optimise during graph partitioning: the higher
375 the value of Q the better the partitioning. If the number of edges within communities exceeds
376 the number of edges expected by chance the value of Q is positive.

377

378 *Community structure*: If nodes of a graph can be easily partitioned into sub-units of densely
379 connected nodes, the graph is presumed to have community structure. This implies that
380 communities merely consist of nodes with more densely connections within and more
381 sparsely connections between communities. This definition only holds true for positive edge
382 weights in the first place. Concerning negative edge weights, the assignment of nodes should
383 be done the opposite way compared to positive edge weights, that is negative edges are sparse
384 within and more dense between communities⁴⁵, a concept evolving from social balance
385 theory⁶³. Although we computed all graph theory metrics using absolute values we cross-
386 checked this limitation by overlaying the community structure for each group on their
387 averaged weighted temporal correlation matrix before converting it to absolute values to
388 verify this issue. As specified before, modularity is an objective function measuring the

389 quality of a graph's community partition. By searching over all possible partitions of a graph,
390 the modularity optimisation method identifies communities that have a high modularity value
391 Q . The detection of a graph's optimal community structure is essential as it may identify
392 functional sub-units so far unknown that influence the overall behaviour of the graph. The
393 optimal community structure is a partition of the graph into non-overlapping sub-units of
394 nodes maximising the number of edges within sub-units and minimising the number of edges
395 between sub-units⁶⁴. One limitation of modularity optimisation is the resolution limit⁴⁴
396 which could lead to failure in resolving even well-defined small communities. Therefore, it
397 might be possible that communities found are clusters of communities in fact. This might be
398 the case if $k_c < \sqrt{2K}$ where k_c denotes the number of internal edges in the community c and K
399 the total number of edges in the graph. Therefore, it is important to look more closely at the
400 internal structure of all communities found as can be done by using the inequation⁴⁴

$$\frac{k_c}{K} - \left(\frac{d_c}{2K}\right)^2 > 0$$

401 with d_c : total degree of nodes in community. If the inequation holds true the community under
402 consideration is actually a single community and not a mixture of two or more smaller ones.
403 All communities found in our analysis comply with the inequation given above. Because
404 community detection using exact modularity optimisation is an NP-hard problem, BCT
405 implemented the Louvain algorithm⁶⁴ which contains a stochastic element that lets the output
406 vary from run to run. To account for this issue, we ran the algorithm a 1000 times per group
407 and used consensus clustering⁶⁵ for selection of best community structure for further
408 computations. Once the community structure of a graph is known, the following two graph
409 theory metrics are easily computed.

410

411 *Within-module degree z score*: The internal organisation of a community or module may vary
412 between totally centralised nodes (one or a few nodes connected to all the others) and totally

413 decentralised ones (all nodes having similar number of edges). Nodes are said to fulfil similar
414 roles if they have similar connectivity within a community. The within-module degree z -score
415 is a metric of how well-connected a node is to other nodes in a community⁴⁶ and is defined as

$$z_i = \frac{k_i(c_i) - \bar{k}(c_i)}{\sigma_{k(c_i)}}$$

416 with c_i : module containing node i , $k_i(c_i)$: within-module degree of i , $\bar{k}(c_i)$: mean of within-
417 module c_i degree distribution and $\sigma_{k(c_i)}$: standard deviation of the within-module c_i degree
418 distribution. The higher the values of z , the higher the within-module degrees are and vice
419 versa which implies that nodes with $z \geq 2.5$ can be classified as hub nodes and nodes with $z <$
420 2.5 as non-hub nodes⁴⁶. Both types of nodes can be subdivided even further by using the
421 values of the participation coefficient P .

422

423 *Participation coefficient*: The two areas in the z -plane (hub and non-hub nodes) can be fine-
424 grained because of the connections of a node to communities other than its own. Sharing the
425 same z -score, one node might be connected to several nodes in other communities while the
426 other might not. The participation coefficient acts as a measure of diversity of inter-modular
427 connections of nodes⁴⁶ and is defined as

$$P_i = 1 - \sum_{j=1}^{n_c} \left(\frac{k_{ij}}{k_i} \right)^2$$

428 with k_{ij} : number of edges of node i to nodes in community j , k_i : total degree of node i and n_c :
429 number of communities detected. The participation coefficient P measures how ‘well-
430 distributed’ the edges of a node are among different communities. It is close to 1 if the edges
431 are uniformly distributed among all the communities and 0 if the entire edges are within its
432 own community.

433

434 *Node topology*: Based on the idea that nodes with the same role should have similar
435 topological properties, the role of a node can be determined by its location in the P - z -
436 parameter plane which defines how the node is positioned in its own community and relative
437 to others. Guimerà and Amaral⁴⁶ defined seven regions by dividing the P - z parameter plane
438 in different areas. Because we are only looking at the tool network, we do not expect to find
439 any hub nodes ($z \geq 2.5$). So, here we only took into account the non-hub nodes area ($z < 2.5$)
440 that was subdivided into four different regions: R1 – nodes with all their edges within their
441 module ($P \leq 0.05$); R2 – nodes with at least 60% of their edges within their module ($0.05 < P$
442 ≤ 0.62); R3 – nodes with half of their edges to other modules ($0.62 < P \leq 0.80$); and R4 –
443 nodes with edges homogeneously distributed among all modules ($P > 0.80$). Such nodes were
444 classified as kinless nodes and are said to be mostly found in network growth models, but not
445 in real-world networks.

446

447 *Distance*: The distance matrix shows the length of shortest paths between all pairs of nodes.
448 Each entry stands for the number of edges that have to be traversed to get from one node to
449 another. By using a weighted correlation matrix, higher correlation coefficients denote shorter
450 distances. We converted the weighted correlation matrices to length by inversion of weights
451 and fed them into Dijkstra algorithm⁶⁶ to compute the distance between nodes.

452

453 **References**

- 454 1. Yavari, F. *et al.* Basic and functional effects of transcranial Electrical Stimulation
455 (tES) – An introduction. *Neurosci Biobehav Rev* **85**, 81 – 92 (2018).
- 456 2. Das, S., Holland, P., Frens, M.A. & Donchin, O. Impact of Transcranial Direct
457 Current Stimulation (tDCS) on Neuronal Functions. *Front Neurosci* **10**, Article 550
458 (2016).

- 459 3. Giordano *et al.* Mechanisms and Effects of Transcranial Direct Current Stimulation.
460 *Dose-Response* **15**, 1 – 22 (2017).
- 461 4. Woods, A.J. *et al.* A technical guide to tDCS, and related non-invasive brain
462 stimulation tools. *Clin Neurophysiol* **127**, 1031 – 1048 (2016).
- 463 5. Almeida, J. *et al.* Polarity-specific transcranial Direct Current Stimulation effects on
464 object-selective neural responses in the Inferior Parietal Lobe. *Cortex* **94**, 176 - 181
465 (2017).
- 466 6. Brunoni, A.R., Fregni, F. & Pagano, R.L. Translational research in transcranial direct
467 current stimulation (tDCS): a systematic review of studies in animals. *Rev Neurosci*
468 **22**, 471 – 481 (2011).
- 469 7. Cappon, D., Jahanshahi, M. & Bisiacchi, P. Value and Efficacy of Transcranial Direct
470 Current Stimulation in the Cognitive Rehabilitation: A Critical Review Since 2000.
471 *Front Neurosci* **10**, Article 157 (2016).
- 472 8. Dedoncker, J., Brunoni, A.R., Baeken, C. & Vanderhasselt, M. A Systematic Review
473 and Meta-Analysis of the Effects of Transcranial Direct Current Stimulation (tDCS)
474 Over the Dorsolateral Prefrontal Cortex in Healthy and Neuropsychiatric Samples:
475 Influence of Stimulation Parameters. *Brain Stimul* **9**, 501 – 517 (2016).
- 476 9. Monti, A. *et al.* Transcranial direct current stimulation (tDCS) and language. *J Neurol*
477 *Neurosurg Psychiatry* **84**, 832 – 842 (2013).
- 478 10. Parkin, B. L., Ekhtiari, H. & Walsh, V. F. Non-invasive Human Brain Stimulation in
479 Cognitive Neuroscience: A Primer. *Neuron* **87**, 932 – 945 (2015).
- 480 11. de Graaf, T. A. & Sack, A. T. Using brain stimulation to disentangle neural correlates
481 of conscious vision. *Front. Psychol* **5**, 1 – 13 (2014).
- 482 12. Saiote, C., Turi, Z., Paulus, W. & Antal, A. Combining functional magnetic resonance
483 imaging with transcranial electrical stimulation. *Front Hum Neurosci* **7**, Article 435
484 (2013).

- 485 13. Vöröslakos, M. *et al.* Direct effects of transcranial electric stimulation on brain circuits
486 in rats and humans. *Nat Commun* **9**, 483 (2018).
- 487 14. Horvath, J.C., Carter, O. & Forte, J.D. Transcranial direct current stimulation: five
488 important issues we aren't discussing (but probably should be). *Front Syst Neurosci* **8**,
489 Article 2 (2014).
- 490 15. Horvath, J.C., Forte, J.D. & Carter, O. Evidence that transcranial direct current
491 stimulation (tDCS) generates little-to-no reliable neurophysiologic effect beyond MEP
492 amplitude modulation in healthy human subjects: A systematic review.
493 *Neuropsychologia* **66**, 213 – 236 (2015).
- 494 16. Horvath, J.C., Carter, O. & Forte, J.D. No significant effect of transcranial direct
495 current stimulation (tDCS) found on simple motor reaction time comparing 15
496 different simulation protocols. *Neuropsychologia* **91**, 544 – 552 (2016).
- 497 17. Mancuso, L.E., Ilieva, I.P., Hamilton, R.H. & Farah, M.J. Does transcranial direct
498 current stimulation improve healthy working memory?: A meta-analytic review. *J*
499 *Cogn Neurosci* **28**, 1063–1089 (2016).
- 500 18. Luft, C.D., Pereda, E., Banissy, M.J. & Bhattacharya, J. Best of both worlds: promise
501 of combining brain stimulation and brain connectome. *Front Syst Neurosci.* **8**, Article
502 32 (2014).
- 503 19. Stagg, C. J. & Nitsche, M. A. Physiological Basis of Transcranial Direct Current
504 Stimulation. *Neuroscientist* **17**, 37 – 53 (2011).
- 505 20. Krause, M.R. *et al.* Transcranial Direct Current Stimulation Facilitates Associative
506 Learning and Alters Functional Connectivity in the Primate Brain. *Curr Biol* **27**, 3086
507 – 3096 (2017).
- 508 21. Filmer, H.L., Dux, P.E. & Mattingley, J.B. Applications of transcranial direct current
509 stimulation for understanding brain function. *Trends Neurosci* **37**, 12 (2014).

- 510 22. Bikson, M., Rahman, A. & Datta, A. Computational Models of Transcranial Direct
511 Current Stimulation. *Clin EEG Neurosci* **43**, 176 – 183 (2012).
- 512 23. Polanía, R., Paulus, W., Antal, A. & Nitsche, M.A. Introducing graph theory to track
513 for neuroplastic alterations in the resting human brain: a transcranial direct current
514 stimulation study. *NeuroImage* **54**, 2287 – 2296 (2011).
- 515 24. Mancini, M. *et al.* Assessing cortical synchronization during transcranial direct current
516 stimulation: A graph-theoretical analysis. *NeuroImage* **140**, 57 – 65 (2016).
- 517 25. Wang, J. *et al.* Test–Retest Reliability of Functional Connectivity Networks During
518 Naturalistic fMRI Paradigms. *Hum Brain Mapp* **38**, 2226 – 2241 (2017).
- 519 26. Bikson, M. & Rahman, A. Origins of specificity during tDCS: anatomical, activity-
520 selective, and input-bias mechanisms. *Front Hum Neurosci* **7**, Article 688, (2013).
- 521 27. Venkatakrisnan, A. & Sandrini, M. Combining transcranial direct current stimulation
522 and neuroimaging: novel insights in understanding neuroplasticity. *J Neurophysiol*
523 **107**, 1 – 4 (2012).
- 524 28. Senço, N.M. *et al.* Transcranial direct current stimulation in obsessive-compulsive
525 disorder: emerging clinical evidence and considerations for optimal montage of
526 electrodes. *Expert Rev Med Devic* **12**, 381 – 391 (2015).
- 527 29. Almeida, J., Fintzi, A. & Mahon, B. Tool manipulation knowledge is retrieved by way
528 of the ventral visual object processing pathway. *Cortex* **49**, 2334 – 2344 (2013).
- 529 30. Hein, G. & Knight, R.T. Superior Temporal Sulcus—It's My Area: Or Is It? *J Cogn*
530 *Neurosci* **20**, 2125 – 2136 (2008).
- 531 31. O'Connell *et al.* Rethinking Clinical Trials of Transcranial Direct Current Stimulation:
532 Participant and Assessor Blinding Is Inadequate at Intensities of 2mA. *PLoS ONE* **7**,
533 e47514 (2012).

- 534 32. Johnson-Frey, S.H., Newman-Norlund, R. & Grafton, S.T. A Distributed Left
535 Hemisphere Network Active During Planning of Everyday Tool Use Skills. *Cereb*
536 *Cortex* **15**, 681 – 695 (2005).
- 537 33. Chen, Q., Garcea, F.E., Almeida, J. & Mahon, B.Z. Connectivity-based constraints on
538 category-specificity in the ventral object processing pathway. *Neuropsychologia* **105**,
539 184 - 196 (2017).
- 540 34. Kristensen, S., Garcea, F.E., Mahon, B.Z. & Almeida, J. Temporal frequency tuning
541 reveals interactions between the dorsal and ventral visual streams. *J Cogn Neurosci*
542 **28**, 1295 – 1302 (2016).
- 543 35. Chao, L.L., Haxby, V.J. & Martin, A. Attribute-based neural substrates in temporal
544 cortex for perceiving and knowing about objects. *Nat Neurosci* **2**, 913 – 919 (1999).
- 545 36. Xia, M., Wang, J. & He, Y. BrainNet Viewer: A Network Visualization Tool for
546 Human Brain Connectomics. *PLoS ONE* **8**, e68910 (2013).
- 547 37. Mazziotta, J. *et al.* A probabilistic atlas and reference system for the human brain:
548 International Consortium for Brain Mapping (ICBM). *Phil Trans R Soc B* **356**, 1293 –
549 1322 (2001).
- 550 38. Meunier, D., Lambiotte, R. & Bullmore, E.T. Modular and hierarchically modular
551 organization of brain networks. *Front Neurosci* **4**, Article 200 (2010).
- 552 39. Zeki, S. & Bartels, A. The autonomy of the visual systems and the modularity of
553 conscious vision. *Phil Trans R Soc B* **353**, 1911 – 1914 (1998).
- 554 40. De Vico Fallani, F., Richiardi, J., Chavez, M. & Achard, S. Graph analysis of
555 functional brain networks: practical issues in translational neuroscience. *Phil Trans R*
556 *Soc B* **369**, 20130521 (2014).
- 557 41. Rubinov, M. & Sporns, O. Complex network measures of brain connectivity: Uses and
558 interpretations. *NeuroImage* **52**, 1059 – 1069 (2010).

- 559 42. He, Y. *et al.* Uncovering Intrinsic Modular Organization of Spontaneous Brain
560 Activity in Humans. *PLoS ONE* **4**, e5226 (2009).
- 561 43. Sporns, O. & Betzel, R.F. Modular Brain Networks. *Annu Rev Psychol* **67**, 613 – 640
562 (2016).
- 563 44. Fortunato, S. & Barthélemy, M. Resolution limit in community detection. *Proc Nat*
564 *Acad Sci USA* **104**, 36 – 41 (2007).
- 565 45. Traag, V.A. & Bruggeman, J. Community detection in networks with positive and
566 negative links. *Phys Rev E* **80**, 036115 (2009).
- 567 46. Guimerà, R. & Nunes Amaral, L.A. Functional cartography of complex metabolic
568 networks. *Nature* **433**, 895 – 900 (2005).
- 569 47. Fertonani, A. & Miniussi, C. Transcranial Electrical Stimulation: What We Know and
570 Do Not Know About Mechanisms. *Neuroscientist* **23**, 109 – 123 (2017).
- 571 48. Fintzi, A.R. & Mahon, B.Z. A Bimodal Tuning Curve for Spatial Frequency Across
572 Left and Right Human Orbital Frontal Cortex During Object Recognition. *Cereb*
573 *Cortex* **24**, 1311 – 1318 (2014).
- 574 49. Macdonald, S.N. & Culham, J.C. Do human brain areas involved in visuomotor
575 actions show a preference for real tools over visually similar non-tools?
576 *Neuropsychologia* **77**, 35 – 41 (2015).
- 577 50. Vingerhoets, G., Acke, F., Vandemaele, P. & Achten, E. Tool responsive regions in
578 the posterior parietal cortex: Effect of differences in motor goal and target object
579 during imagined transitive movements. *NeuroImage* **47**, 1832 – 1843 (2009).
- 580 51. Peeters, R.R., Rizzolatti, G. & Orban, G.A. Functional properties of the left parietal
581 tool use region. *NeuroImage* **78**, 83 – 93 (2013).
- 582 52. Creem-Regehr, S.H. & Lee, J.N. Neural representations of graspable objects: are tools
583 special? *Cognitive Brain Res* **22**, 457 – 469 (2005).

- 584 53. Eickhoff, S. *et al.* A new SPM toolbox for combining probabilistic cytoarchitectonic
585 maps and functional imaging data. *NeuroImage* **25**, 1325 – 1335 (2005).
- 586 54. Talairach, P. & Tournoux, J. *Co-Planar Stereotaxic Atlas of the Human Brain*
587 (Thieme, 1988).
- 588 55. Rubinov, M. & Sporns, O. Weight-conserving characterization of complex functional
589 brain networks. *NeuroImage* **56**, 2068 – 2079 (2011).
- 590 56. Corey, D.M, Dunlap, W.P. & Burke, M.J. Averaging Correlations: Expected Values
591 and Bias in Combined Pearson's r s and Fisher's z Transformation. *J Gen Psychol* **125**,
592 245 – 261 (1998).
- 593 57. Olkin, I. & Pratt, J. W. Unbiased estimation of certain correlation coefficients. *Ann*
594 *Math Stat* **29**, 201 – 211 (1958).
- 595 58. Zimmerman, D.W., Zumbo, B.D. & Williams, R.H. Bias in Estimation and
596 Hypothesis Testing of Correlation. *Psicológica* **24**, 133 – 158 (2003).
- 597 59. Alexander, R.A. A note on averaging correlations. *B Psychonomic Soc* **28**, 335 – 336
598 (1990).
- 599 60. van Wijk, B.C.M., Stam, C.J. & Daffertshofer, A. Comparing Brain Networks of
600 Different Size and Connectivity Density Using Graph Theory. *PLoS ONE* **5**, e13701
601 (2010).
- 602 61. Phillips, D.J. *et al.* Graph theoretic analysis of structural connectivity across the
603 spectrum of Alzheimer's disease: The importance of graph creation methods.
604 *NeuroImage: Clinical* **7**, 377 – 390 (2015).
- 605 62. Newman, M.E.J. Analysis of weighted networks. *Phys Rev E* **70**, 056131 (2004).
- 606 63. Harary, F. On the notion of balance of a signed graph. *Mich Math J* **2**, 143 – 146
607 (1953).
- 608 64. Blondel, V.D, Guillaume, J.-L., Lambiotte, R. & Lefebvre, E. Fast unfolding of
609 communities in large networks. *J Stat Mech-Theory E* **2008**, P10008 (2008).

610 65. Lancichinetti, A. & Fortunato, S. Consensus clustering in complex networks. *Sci Rep*
611 2, 336 (2012).

612 66. Dijkstra, E.W. A Note on Two Problems in Connexion with Graphs. *Numer Math* 1,
613 269 – 271 (1959).

614

615 **Acknowledgements**

616 This research was supported by a Foundation for Science and Technology of Portugal and
617 Programa COMPETE grant (PTDC/ MHC-PCN/0522/2014) to J.A. M.R. and J.A. were
618 supported by Deutscher Akademischer Austauschdienst (Projekt-ID 57212180) and CRUP.
619 S.K. is supported by a Foundation for Science and Technology of Portugal and Programa
620 COMPETE grant (PTDC/MHC-PCN/0522/2014). This research was supported by German
621 Research Foundation grant SCHA 546/22-1 to L.R.S.

622

623 **Author contributions**

624 M.R. performed data analyses, prepared the graphics and wrote the paper. S.K. performed
625 data analysis. L.R.S. contributed ideas. J.A. conceived and designed the project, and critically
626 revised the manuscript. M.R. and J.A. interpreted the data.

627

628 **Conflicts of interest**

629 All authors declare no conflict of interest.

Table 1. Overview of brain regions in analysed functional network

Lobe	Hemisphere	Structure	Brodmann area [BA]	Label	Talairach Coordinates		
					X	Y	Z
ROIs of Tool Network							
temporal	left	posterior middle temporal gyrus	BA 37	pMTG	-42	-62	-7
temporal	left	middle fusiform gyrus	BA 37	MFG	-24	-48	-8
occipital	left	extrastriate visual cortex	BA 19	V3aV7	-23	-80	24
occipital	right	extrastriate visual cortex	BA 19	V3aV7	25	-78	27
parietal	left	anterior angular gyrus	BA 39	PGa	-41	-63	33
occipital	left	posterior angular gyrus	BA 39	PGp	-40	-73	24
parietal	left	superior parietal lobe (anterior parts)	BA 7	BA7a	-18	-64	49
	right				18	-65	50
parietal	left	superior parietal lobe (posterior parts)	BA 7	BA7p	-10	-76	40
	right				13	-76	44
parietal	left	lateral superior parietal lobe	BA 7	7PC	-31	-55	50
parietal	right	lateral superior parietal lobe	BA 7	7PC	27	-54	49
parietal	left	supramarginal gyrus	BA 40	PF	-53	-41	31
temporal	left	supramarginal gyrus	BA 40	PFcm	-45	-39	21
parietal	left	supramarginal gyrus	BA 40	PFm	-48	-54	34
parietal	left	supramarginal gyrus	BA 40	PFop	-53	-28	24
parietal	left	supramarginal gyrus	BA 40	PFt	-48	-29	33
parietal	left	intraparietal sulcus	BA 7/40	hIP1	-34	-52	34
parietal	left	intraparietal sulcus	BA 7/40	hIP2	-42	-44	37
parietal	left	superior parietal lobe	BA 7/40	hIP3	-29	-54	38
Stimulation Sites							
parietal	left	inferior parietal lobe	BA 40	IPL	-38	-37	36
temporal	right	superior temporal sulcus	BA 37	STS	44	-45	6

631 Here, we list the names of the brain areas, labels used in the text and centre coordinates (x,y,z)
632 in Talairach space of the regions of interests (ROI) of the tool network and the stimulation
633 sites. The anterior and posterior parts of the superior parietal lobe are bilateral ROIs.